Journal of New Materials for Electrochemical Systems 19, 217-222 (2016)

Lead Corrosion and Formation of Lead Oxides from a Lead-air Cell in Methanesulfonic Acid

Wan Jeffrey Basirun[1,2,*], Idris Mohamed Saeed[3], Hanieh Ghadimi[2], Magaji Ladan[2] Mohammad Reza Mahmoudian[4], Mehdi Ebadi[5], Lukman Bola Abdulrauf[2], Zulkarnain Endut[6]

[1]Institute of Nanotechnology & Catalysis Research (NanoCat), Institute of Postgraduate Studies, University Malaya, 50603 Kuala Lumpur, Malaysia.
[2]Department of Chemistry, University Malaya, Kuala Lumpur 50603, Malaysia.
[3]Department of Chemical Engineering, Faculty of Engineering, University of Malaya, Kuala Lumpur 50603, Malaysia
[4]Department of Chemistry, Shahid Sherafat, University of Farhangian, 15916, Tehran, Iran.
[5]Department of Chemistry, Faculty of Sciences, Islamic Azad University, Gorgan, 49147-39975 Iran.
[6]Center of Foundation Studies, Faculty of Science, Universiti Putra Malaysia, 43400 UPM Serdang, Selangor, Malaysia.

Received: January 20, 2016, Accepted: October 15, 2016, Available online: November 29, 2016

Abstract: *The corrosion of lead in methanesulfonic acid solution in the presence of a MnO_2 air cathode in a primary lead-air cell is investigated. The highest power density of the lead-air cell is 2.8 mW cm^{-2}. X-ray photoelectron spectroscopy and powder X-ray diffraction results demonstrate the formation of lead (II) oxide and lead (IV) dioxide on the air cathode after continuous discharge. Field emission scanning electron microscopy image shows that the surface coverage of lead (II) oxide and lead (IV) dioxide on the air cathode is only partial and will allow oxygen reduction.*

Keywords: anodic dissolution; X-ray photoelectron spectroscopy; lead-air cell; lead oxides

1. INTRODUCTION

Lead is a commonly available and highly corrosion-resistant metal that is often used as the negative electrode in lead-acid secondary batteries where the formation of insoluble $PbSO_4$ during discharge terminates the cell operation. Despite the environmental problems associated with lead compounds, lead-acid batteries continue to be used in automobiles because of their large sales value, amounting to an estimated 30 billion US dollar each year. Lead corrosion by methanesulfonic acid in a secondary lead flow-battery with a soluble lead negative electrode and a lead (IV) dioxide positive electrode in methanesulfonic acid solution has been reported and further exemplifies the importance of lead in energy storage devices [1, 2]. Oxygen reduction is an important process, particularly in metal-air batteries and fuel cells. Oxygen reduction takes place at the air cathode to complete the electrochemical reaction of the cell and generate electricity. Due to the slow kinetics of the oxygen reduction reaction, several compounds have been used as electro-catalysts. Highly dispersed platinum metal is an excellent electro-catalyst for oxygen reduction, but the cost of platinum hinders large-scale manufacturing. Various types of material has been used as air cathodes in metal-air batteries and fuel cells, but currently manganese dioxide compounds are the most widely used electro-catalysts in metal-air batteries and fuel cells, as they are readily available from manufacturers. In this work, lead corrosion and the surface formation of lead oxides at air cathode in a lead-air cell in methanesulphonic acid solution are investigated; this cell is an undivided primary metal-air cell using a lead negative electrode and a manganese dioxide air cathode.

*To whom correspondence should be addressed: Email: wjbasirun@gmail.com
Phone: 603 7967 4082, Fax: 603 7967 4193

2. EXPERIMENTAL METHODS

Lead foil (99.9%) was procured from Goodfellow Cambridge Limited, and methanesulfonic acid (99.9%) was procured from Sigma Aldrich. The air cathode was fabricated from catalytic manganese dioxide (MnO_2) powder mixed with small amounts of carbon black powder to increase the conductivity. The catalytic powders were pressed onto a nickel mesh current collector on both

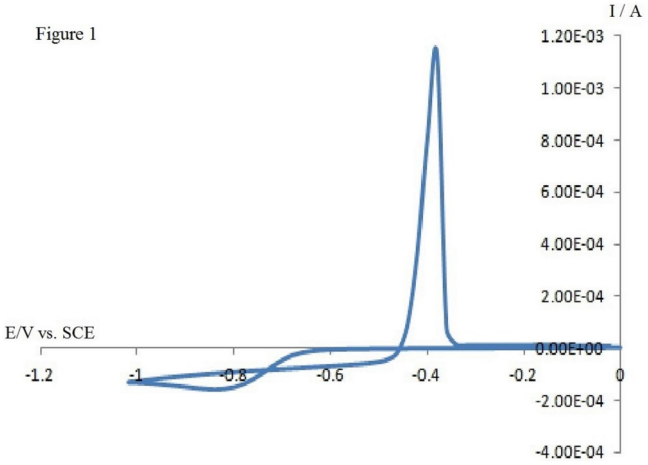

Figure 1. Cyclic voltammetry of 4.5 mM $Pb(CH_3COO)_2$ in 1.5 M CH_3SO_3H on a glassy carbon working electrode (WE) of 2 mm in diameter at 25 mV s^{-1}.

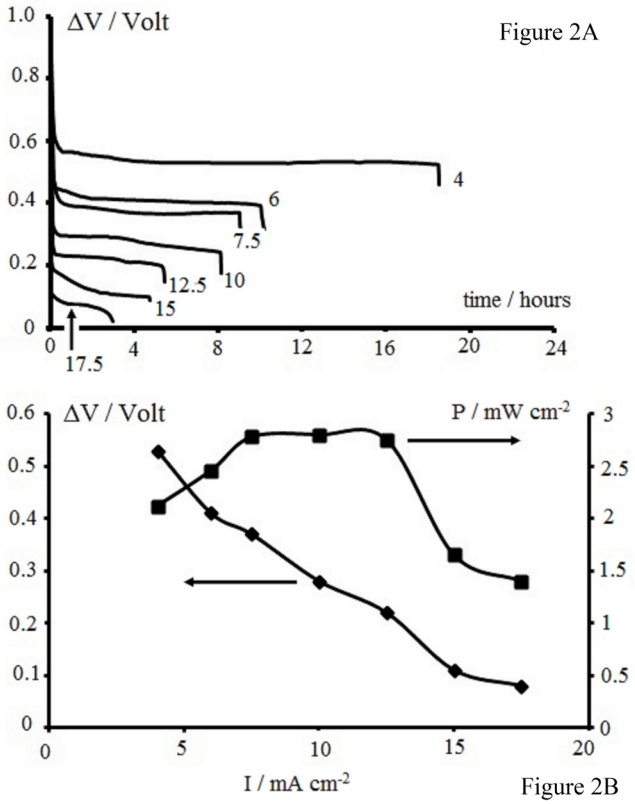

Figure 2. A) Discharge profiles at different constant current densities. B) I-V-P plot of the lead-air cell.

sides, with one side attached to a Teflon membrane which is permeable to air but not the electrolyte. The air cathode used in these experiments had a diameter of 0.9 cm, and the surface area of lead exposed to the electrolyte was 1 cm^2. The schematic diagrams of the air cathode and the cell casing are described elsewhere [3, 4]. Oxygen is readily available from the atmosphere, and no forced air flow towards the air cathode was used in these experiments. Cyclic voltammetry (CV) was carried out using a potentiostat /galvanostat (Autolab model PGSTAT-302N, Ecochemie, Utrecht, Netherlands). General-purpose electrochemical software (GPES) installed in the computer and interfaced with a Universal Serial Bus card (USB_IF030), was used to run the CV experiments. The experiments were conducted using a single-compartment electrochemical cell, with a 2 mm diameter glassy carbon (GC) as the working electrode, a saturated calomel electrode (SCE) as the reference and a graphite rod as the counter electrode. Open circuit potential (OCP) and cell discharge experiments were carried out using a Won A-Tech WBCS 3000 (Korea Republic) battery cycler instrument. All experiments were carried out at room temperature, 300 K (27 °C). Powder X-ray diffraction (XRD) and field emission scanning electron microscopy (FESEM) were used to analyze the air cathode surface before and after discharge. The XRD experiments were conducted using a Siemens D5000 instrument, while FESEM was conducted using a FEI Quanta 200F instrument. X-ray photoelectron spectroscopy (XPS) was conducted using a Kratos Analytical Axis Ultra instrument with an Al K_α radiation source of 253.6 eV with a spectral resolution of 0.1 eV, and this technique was used to analyze the air cathode surface after cell discharge.

3. RESULTS AND DISCUSSIONS

3.1. CV and OCP measurements

Figure 1 shows the CV for a solution of 4.5 mM $Pb(CH_3COO)_2$ in 1.5 M CH_3SO_3H on a GC working electrode at 25 mV s^{-1} scan rate. Lead is electrodeposited on the GC surface; the resultant peak occurs at -0.82 V vs. SCE in the forward scan. In the reverse scan, lead electrodeposition on the GC surface occurs until an oxidation peak is observed at -0.40 V vs. SCE, where all of the deposited lead is oxidized into the solution. The electrodeposition of Pb^{2+} in methanesulfonic acid is a diffusion-controlled process with a diffusion coefficient of 6.1 x 10^{-10} m^2 s^{-1} [2]. Figure 1 shows that the oxidation peak is higher and sharper than the reduction wave. The deposition of the Pb^{2+} occurs on glassy carbon electrode (GCE) in the cathodic scan, which requires activation energy due to the nucleation phenomena, as lead is electrodeposited onto a foreign substrate [1, 2]. Therefore the deposition will occur at more negative potentials (around -0.65 V, Fig. 1) compared to the oxidation peak. In the reverse anodic scan, the electrodeposition of Pb^{2+} will continue until -0.45 V. At potentials more positive than -0.45 V, the oxidative stripping of Pb from the GCE occurs with a large peak at -0.40 V. The oxidation of Pb to Pb^{2+} produces a large sharp peak at -0.40 V because the process is not limited by diffusion, unlike the electroreduction of Pb^{2+} on the cathodic scan which shows reduction waves. The combination of the both cathodic and anodic scans produces a typical loop seen in Fig. 1, if the process involves a nucleation phenomenon, i.e. electrodeposition of a material onto a foreign substrate [1, 2].

The OCP measurements for 24 hours for the lead-air primary cell in 1.5 M methanesulfonic acid gave values from 1.15 to 1.20 V. The oxidation of lead to Pb^{2+} has the standard potential:

$$Pb^{2+} + 2e^- \rightarrow Pb \qquad E^{\Theta} \text{ (V vs. SHE)} = -0.13 \qquad (1)$$

Oxygen reduction at the MnO_2 air electrode in acidic solutions depends on the acid concentration and has the standard potentials [5]:

$$O_2 + H^+ + 2e^- \rightarrow HO_2^- \qquad E^\Theta \text{ (V vs. SHE)} = 0.34 \qquad (2)$$

$$O_2 + 2H^+ + 2e^- \rightarrow H_2O_2 \qquad E^\Theta \text{ (V vs. SHE)} = 0.68 \qquad (3)$$

The most probable reaction at the air cathode in 1.5 M methanesulfonic acid is represented by eq. 3, and this reaction occurs at higher acid concentrations. Unlike in the alkaline medium, the ORR in acidic medium proceeds with a 2-electron mechanism (eq. 3). This is followed by the further reduction of the H_2O_2:

$$H_2O_2 + 2H^+ + 2e^- \rightarrow 2H_2O \qquad (4)$$

However this reaction (eq. 4) is unlikely, due to the instability of the hydrogen peroxide towards disproportion reaction [6]:

$$Pb^{2+} + 2e^- \rightarrow Pb \qquad E^\Theta \text{ (V vs. SHE)} = -0.13 \qquad (5)$$

The synthesis of hydrogen peroxide from dissolved oxygen in acidic solutions has also been reported [7].

3.2. Cell performance

The cell notation for the undivided primary lead-air cell can be represented as Pb / 1.5 M CH_3SO_3H / MnO_2 air cathode. Figure 2a shows the discharge profiles at constant current densities of 4, 6, 7.5, 10, 12.5, 15 and 17.5 mA cm^{-2}. The cell is discharged until the lead negative electrode is completely dissolved. Table 1 presents some parameters calculated from the weight loss measurements of the lead before and after discharge and other parameters calculated based on the discharge profiles presented in Fig. 2a. An example of the calculation in Table 1 is as follows. A discharge current of 10 mA and a total time of 8.27 hrs (C1, row 5) is equivalent to a total discharge capacity of 82.7 mAh (C5). From the Faraday equation It = mnF, the Faradaic equivalent of 82.7 mAh (It in the Faraday equation) is 1.54 x 10^{-3} mol (C4, m in Faraday equation), where n = 2 for the dissolution of Pb. The experimental weight loss of the lead foil at 10 mA current is estimated as 1.68 x 10^{-3} mol (C2). The Faradaic equivalent of this weight loss is 90.06 mAh (C3), from the Faraday equation. But the experimental weight loss of the lead anode is due to the electrochemical oxidation (C5) and the chemical oxidation by hydrogen peroxide (eq. 4) in the solution, and is always higher than the electrochemical oxidation (C5) of the lead from Fig. 2A. Therefore C3 is always higher than C5, and the ratio of C5 to C3 is the Faradaic efficiency of the discharge. The discharge capacities calculated from the weight loss measurements are always higher than the discharge capacities calculated from Fig. 2a. This result could be due to the formation of hydrogen peroxide at the air cathode as described by eq. 3. The oxidation of lead in the presence of dissolved oxygen occurs through the initial equation:

$$O_2 + 4H^+ + 2Pb \rightarrow 2Pb^{2+} + 2H_2O \qquad (6)$$

And proceeds in the presence of hydrogen peroxide:

$$2H^+ + H_2O_2 + Pb \rightarrow 2Pb^{2+} + 2H_2O \qquad (7)$$

This observation is also in accordance with a decrease in the charge efficiency of a lead (II) flow-battery to 77% after 65 cycles when hydrogen peroxide is added [8].

Table 1 also shows longer discharge times gave lower Faradaic efficiency for the dissolution of lead. This result could be due to the hydrogen peroxide formation from the air cathode, which has sufficient time to diffuse to the lead negative electrode and dissolve it according to eq. 4. Figure 2b presents I-V-P plots from the discharge profiles (Fig. 2a) which gives the highest power density of 2.8 mW cm^{-2}. Although the electrochemical equivalent of lead (259 Ah kg^{-1}) as a metal-air primary cell is quite low compared to zinc (820 Ah kg^{-1}) and aluminum (2978 Ah kg^{-1}), the dissolution of lead in methanesulfonic acid does not suffer from surface passivation, unlike zinc-air and aluminum-air cells.

The concentration of Pb^{2+} ions in solution from each discharge current can be monitored using voltammetry and estimated from the Randles-Sevchik equation:

$$I = 0.4463nF\left(\frac{nF}{RT}\right)^{1/2} AcD^{1/2}v^{1/2} \qquad (8)$$

The plot of I vs. $v^{1/2}$ allows the Pb^{2+} concentration in the solution after cell discharge to be estimated using the Pb^{2+} diffusion coefficient in methanesulfonic acid (D = 6.1 x 10^{-10} m^2 s^{-1} [2]). Figure 3a presents voltammograms of the lead solution from a 15 mA cm^{-2} discharge current, and Fig. 3b presents a plot of I vs. $v^{1/2}$. Table 2 presents the estimated mole fraction of lead in the solution and the estimated mole fraction of lead deposited on the air cathode after cell discharge. As can be observed from Table 2, there is no obvious trend for the amount of Pb^{2+} present in solution and the lead deposited on the air cathode with the increase of discharge current

Table 1. Some calculated parameters based on weight loss measurements and based on the discharge (E vs. t) profile presented in Figure 2A.

C1. Discharge current and total dicharge time in Fig. 2 / mA, hrs	C2. Experimental weight loss / 10^{-3} mol	C3. Discharge capacity from experimental weight loss measurements / mAh	C4. Calculated Faradaic weight loss in Fig. 2 / 10^{-3} mol	C5. Discharge capacity from Fig. 2 / mAh	(C5/C3). Faradaic efficiency for discharge / %
17.5, 3.00	0.99	53.08	0.98	52.50	99
15, 5.25	1.51	80.95	1.47	78.75	97
12.5, 5.42	1.35	72.37	1.26	67.75	93
10, 8.27	1.68	90.06	1.54	82.70	92
7.5, 9.93	1.51	81.13	1.39	74.48	92
6, 10.17	1.25	67.05	1.14	61.02	91
4, 18.53	1.52	81.46	1.38	74.13	91

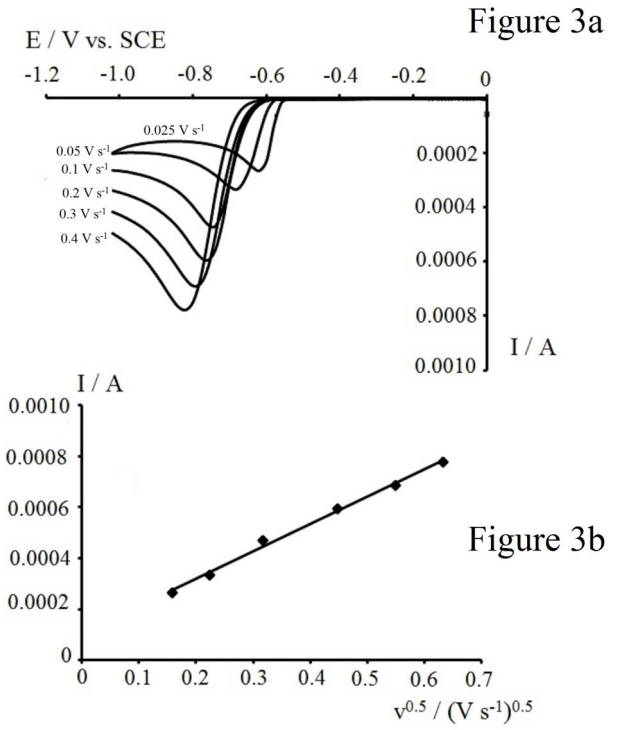

Figure 3. A) Voltammograms of a Pb^{2+} solution using a 15 mA cm^{-2} discharge current. B) A plot of I vs. $v^{1/2}$ of a Pb^{2+} solution.

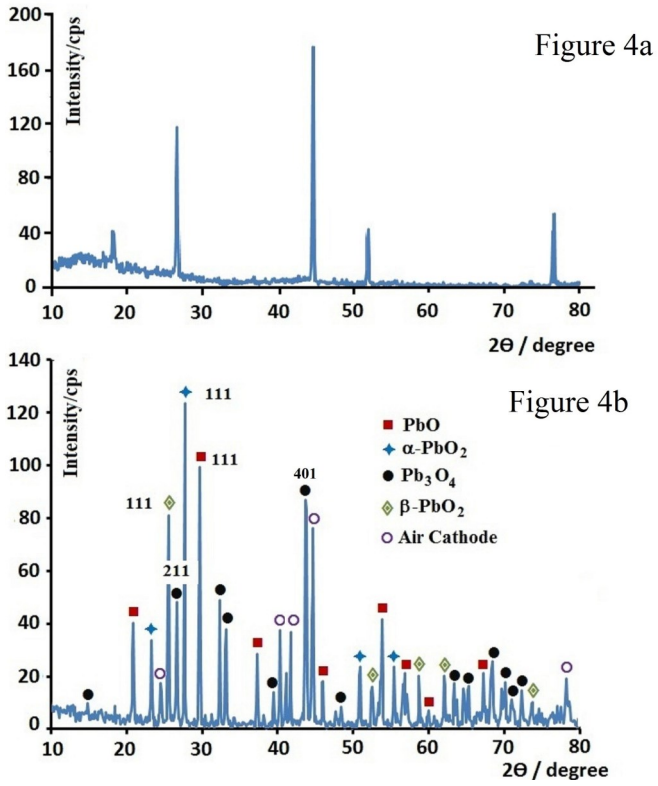

Figure 4. A) XRD of the air cathode before discharge. B) XRD of the air cathode after continuous discharge.

because the deposited PbO and PbO_2 on the air cathode can re-dissolve into the solution as follows:

$$PbO + 2H^+ + 2e^- \rightarrow Pb^{2+} + H_2O \quad (9)$$

$$PbO_2 + 4H^+ + 2e^- \rightarrow Pb^{2+} + 2H_2O \quad (10)$$

Equation 7 is the discharge reaction of the PbO_2 positive electrode in the lead-lead dioxide flow-battery in methanesulfonic acid solution [2].

3.3. XRD of the air cathode

Figure 4a shows the XRD of the air cathode before discharge. The air cathode used in the XRD (Sec. 3.3), FESEM and XPS (Sec. 3.4) results was from continuous discharge experiments with current densities from 4 mA cm^{-2} to 17.5 mA cm^{-2}. The XRD was taken from the as-deposited lead oxides on the MnO_2 air cathode. The diffractogram of the air cathode before discharge has 2θ angles: 18.5°, 24.5°, 44.6°, 52°, and 77°. The 2θ angle of 18.5° is attributed to fibrous carbon-MnO_2 material, while the angles of 44.6°, 52°, and 77° are attributed to the nickel mesh in the air cathode [3, 4]. The 2θ angle of 24.5° is attributed to graphite, and the angle of 44.6° is also due to the MnO_2 material [9]. Figure 4b shows the XRD of the air cathode after continuous discharge where the 2θ angles with the strongest intensity for PbO, PbO_2 and Pb_3O_4 ($PbO.PbO_2.PbO$) are all present. Comparison of the 2θ angles in Fig. 4b are done with the Joint Committee on Powder Diffraction Standards (JCPDS) file numbers of 072-0094, 073-0532, 072-2440, and 075-2417 for PbO, Pb_3O_4, α-PbO_2 and β-PbO_2, respectively. The 2θ angles with the strongest intensities for PbO, α-PbO_2, β-PbO_2 occur at 29.5°, 28.5°and 25.4° respectively, while Pb_3O_4 occurs at 26.3° and 401°, are marked with their respective lattice planes in Fig. 4b, which are close to the values reported in the JCPDS data. Hydrogen peroxide is an oxidizing agent capable of oxidation on the air cathode, where the formation of lead (II) oxide and lead (IV) dioxide on the air cathode can be represented as follows:

$$Pb^{2+} + H_2O_2 + 2e^- \rightarrow PbO + H_2O \quad (11)$$

$$Pb^{2+} + 2H_2O_2 + 2e^- \rightarrow PbO_2 + 2H_2O \quad (12)$$

Anodic deposition of lead (IV) dioxide in methanesulfonic acid

Table 2. Estimated mol fraction of lead in solution and lead on the air cathode for each discharge current in Figure 2A.

Discharge current / mA cm^{-2}	Mol fraction of Pb in solution	Mol fraction of Pb on air cathode
17.5	0.42	0.58
15	0.49	0.51
12.5	0.41	0.59
10	0.49	0.51
7.5	0.47	0.53
6	0.41	0.59
4	0.45	0.55

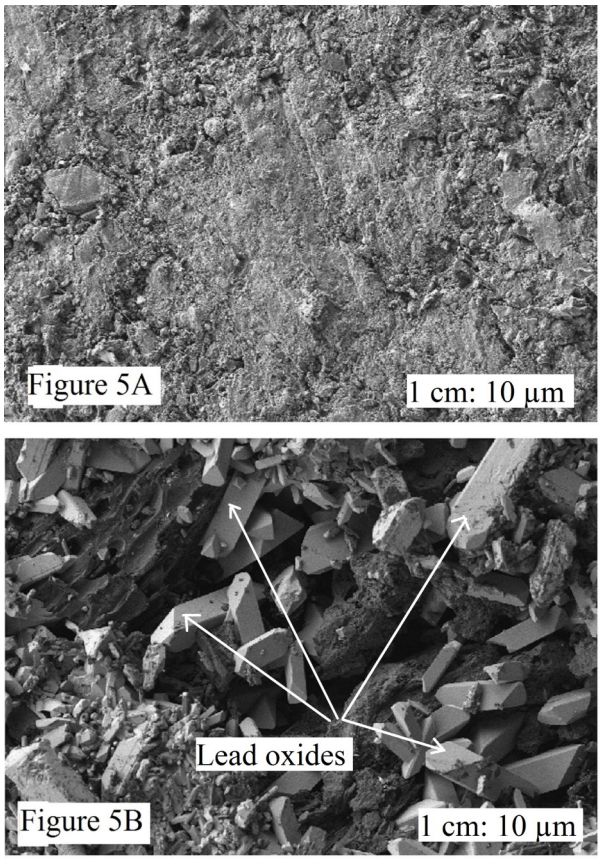

Figure 5. A) FESEM image (500X) of the air cathode before continuous discharge. B) FESEM image (500X) of the air cathode after continuous discharge.

solution has also been reported [10]. But in this work, the formation of lead (II) oxide and lead (IV) dioxide on the air cathode occur by cathodic deposition, unlike in previous reports of lead (IV) dioxide deposition, where anodic deposition was observed. During discharge, there was no formation of precipitates in the bottom of the cell, therefore it is unlikely that the lead oxide formation occurred via chemical precipitation in the solution. Moreover, the dissolution of the lead negative electrode and the formation of lead (II) oxide and lead (IV) dioxide on the surface of the air cathode are quite similar to the situation in lithium-air batteries. Powder XRD studies on lithium-air batteries have shown that the dissolved lithium negative electrode forms lithium oxide (Li_2O_2) on the air cathode after cell discharge [11]. The 2θ angles at 40.3, 41.1 and 41.7 in Fig. 4b are attributed to the formation of MnOOH [12], which is not present in the XRD of the air cathode before discharge in Fig. 4a. The MnOOH is a stable intermediate that is formed during oxygen reduction on the air cathode in alkaline solution; the reaction for this process can be written as follows [13]:

$$MnO_2 + H_2O + e^- \rightarrow MnOOH + OH^- \quad (13)$$

In acidic solution the reaction can be written as:

$$MnO_2 + H^+ + e^- \rightarrow MnOOH \quad (14)$$

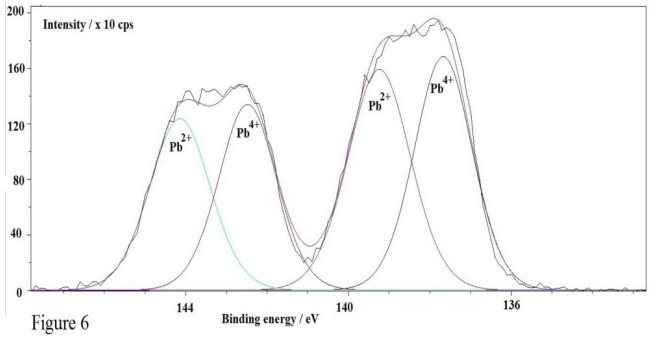

Figure 6. XPS spectrum of Pb 4f levels for the air cathode after continuous discharge.

3.4. FESEM and XPS of air cathode

Figure 5a and 5b are FESEM images of the air cathode before and after discharge, respectively. Figure 5a shows the surface of the MnO_2 air cathode. Apparently, crystallized MnO_2 are absent from the surface, due to the high pressure pressing during the fabrication process. In Fig. 5b, deposited lead oxides can be observed as light grey cubical shapes on the dark MnO_2 substrate. The formation of cubical lead oxides (Fig. 5b) is quite different from previous reports of anodic electrodeposition of lead dioxides. Other researchers have reported cauliflower shapes [14], sharp grains [10], serrated teeth [15], thin sheets [16] and feather-like microstructures [17]. The type of solution, deposition conditions, substrates and additives used clearly influence the surface morphology of the deposited lead oxide coatings [18, 19]. Surface deposits exhibiting cauliflower-type morphology with a circular diameter of approximately 0.5 mm have also been reported [20]. From the FESEM image in Fig. 5b, full surface coverage of the lead oxides on the air cathode did not occur. The formation of lead oxides on the air cathode allows gaps and holes where oxygen reduction reaction could still occur.

XPS was carried out on the air cathode to determine the valence state of the lead oxide deposits. Figure 6 presents the XPS spectrum

Table 3. Comparisons between the different binding energies of $4f_{7/2}$ and $4f_{5/2}$ for the Pb (II) and Pb (IV) oxidation states with results from other researchers.

Oxidation states	Binding energy $4f_{7/2}$ (eV)	Binding energy $4f_{5/2}$ (eV)	References
Pb (IV)	137.7	142.5	This work
	137.4	-	21
	136.9	141.8	22
	137.9	-	23
Pb (II)	139.2	144.1	This work
	138.1	-	21
	138.8	143.1	22
	138.9	-	23

of the air cathode after continuous discharge experiments. From the curve fitting, the XPS spectrum shows peaks at two regions, 141-146 eV (for Pb $4f_{5/2}$) and 135-141 eV (for Pb $4f_{7/2}$). Deconvolution of the two regions using Gaussian fitting demonstrates the presence of Pb^{4+} and Pb^{2+} peaks with a ratio close to one. The data are tabulated in Table 3, and the results obtained compare well with data in the literature [21, 22, 23].

4. CONCLUSION

A primary metal-air cell with a soluble lead negative electrode and an air cathode in methanesulfonic acid solution was successfully tested. The highest power density obtained is 2.8 mW cm^{-2}. The oxidation of the lead negative electrode did not exhibit 100% current efficiency. The formation of hydrogen peroxide at the air cathode during discharge could have caused the non-Faradaic dissolution of the lead negative electrode, which contributes to the lower discharge capacity of the lead-air cell. XRD demonstrates the formation of PbO, Pb_3O_4, α-PbO_2 and β-PbO_2 on the air cathode after continuous discharge. FESEM imaging shows cubical lead (II) oxide and lead (IV) dioxide shapes where full surface coverage of the lead oxides on the air cathode did not occur; this insufficient surface coverage would allow oxygen reduction to continue on the air cathode. The XPS results also show that the oxidation states of the lead oxides are Pb (II) and Pb (IV), and these oxidation states are formed in nearly equal amounts.

5. ACKNOWLEDGEMENTS

The authors would like to thank University of Malaya and Ministry of Higher Education, for providing financial assistance with grant numbers FP033 2013A, PG015-2013A and PG-084-2013A.

REFERENCES

[1] A. Hazza, D. Pletcher and R. Willis, Phys. Chem. Chem. Phys., 6, 1773 (2004).
[2] D. Pletcher and R. Willis, Phys. Chem. Chem. Phys., 6, 1779 (2004).
[3] R. Othman, W.J. Basirun, A.H. Yahya and A.K. Arof, J. Power Sources, 103, 34 (2001).
[4] A.A. Mohamad, J. Power Sources, 159, 752 (2006).
[5] V.G. Khomenko, V.Z. Barsukov and A.S. Katashinskii, Electrochim. Acta, 50, 1675 (2005).
[6] S.K. Bikkarolla, P. Cumpson, P. Joseph and P. Papakonstantinou, Faraday Discuss., 173, 415 (2014).
[7] Z. Qiang, J.H. Chang and C.P. Huang, Water Res., 36, 85 (2002).
[8] J. Collins, X. Li, D. Pletcher, R. Tangirala, D.S. Campbell, F.C. Walsh and C. Zhang, J. Power Sources, 195, 2975 (2010).
[9] Y.L. Cao, H.X. Yang, X.P. Ai and L.F. Xiao, J. Electroanal. Chem., 557, 127 (2003).\
[10] A.B. Velichenko, R. Amadelli, E.V. Gruzdeva, T.V. Luk'yanenko and F.I. Danilov, J. Power Sources, 191, 103 (2009).
[11] C.O. Laoire, S. Mukerjee, E.J. Plichta, M.A. Hendrickson and K.M. Abraham, J. Electrochem. Soc., 158, A302 (2011).
[12] Y.C. Zhang, T. Qiao and X.Y. Hu, J. Solid State Chem., 177, 4093 (2004).
[13] Y.L. Cao, H.X. Yang, X.P. Ai and L.F. Xiao, J. Electroanal. Chem., 557, 127 (2003).
[14] D. Devilliers, M.T.D. Thi, E. Mahé, V. Dauriac and N Lequeux, J. Electroanal. Chem., 573, 227 (2004).
[15] Y. Mohammad and D. Pletcher, Electrochim. Acta, 52, 786 (2006).
[16] P. Veluchamy and H. Minoura, Appl. Surf. Sci., 126, 241 (1998).
[17] C.T.J. Low, D. Pletcher and F.C. Walsh, Electrochem. Commun., 11, 1301 (2009).
[18] A. Hazza, D. Pletcher and R. Wills, J. Power Sources, 149, 103 (2005).
[19] D. Pletcher, H. Zhou, G. Kear, C.T.J. Low, F.C. Walsh and R.G.A. Wills, J. Power Sources, 180, 621 (2008).
[20] D. Pletcher, H. Zhou, G. Kear, C.T.J. Low, F.C. Walsh and R.G.A. Wills, J. Power Sources, 180, 630 (2008).
[21] H.A. Samad and P.R. Watson, Appl. Surf. Sci., 136, 46 (1998).
[22] M.M. Rahman, K.M. Krishna, T. Soga, T. Jimbo and M. Ume, J. Phys. Chem. Solids, 60, 201 (1999).
[23] K.S. Kim, T.J. O'Leary and N. Winograd, Anal. Chem., 45, 2214 (1973).